We are IntechOpen, the world's leading publisher of Open Access books
Built by scientists, for scientists

6,900
Open access books available

186,000
International authors and editors

200M
Downloads

154
Countries delivered to

Our authors are among the

TOP 1%
most cited scientists

12.2%
Contributors from top 500 universities

BOOK CITATION INDEX
CLARIVATE ANALYTICS
INDEXED

WEB OF SCIENCE™

Selection of our books indexed in the Book Citation Index
in Web of Science™ Core Collection (BKCI)

Interested in publishing with us?
Contact book.department@intechopen.com

Numbers displayed above are based on latest data collected.
For more information visit www.intechopen.com

Parametric Interaction of VLF and ELF Waves in the Ionosphere

Vladimir I. Sotnikov

Abstract

In this Chapter we analyze a non-linear parametric interaction between Very Low Frequency (VLF) and Extremely Low Frequency (ELF) waves in the ionosphere. We demonstrate that nonlinear parametric coupling between quasi-electrostatic Lower Oblique Resonance (LOR) and ELF waves significantly contributes to the VLF electromagnetic whistler wave spectrum. Analytical and numerical results are compared with experimental data obtained during active space experiments and satellite data. These data clearly show that presence of VLF waves in the region of plasmasphere boundary layer, where there are no injected due to substorm/storm activity energetic electrons with energies of tens keV can strongly affect the radiation belt boundary.

Keywords: Ionosphere, wave interaction, whistlers

1. Introduction

The generation of VLF sideband emissions due to parametric interaction of LOR and ELF waves was first suggested in [1, 2] in an attempt to explain an experimental results observed in the ionosphere by the Aureol 3 satellite [3, 4] and during the CHARGE 2B ionospheric rocket experiment [5]. Sideband VLF wave emissions can be explained as secondary peaks above and below the primary peak. They results from parametric interaction of excited VLF and ELF waves. Next, nonlinear parametric interactions between quasi-electrostatic LOR and ELF waves was proposed as possible generation mechanisms of VLF whistler waves in the Turbulent Plasmosphere Boundary Layer (TPBL). Excitation of these waves was analyzed through an assessment of observations from the Cluster spacecraft and Van Allen Probes [6]. To further validate a model developed in [1, 2] and adapted in [6] to explain the observations of whistler waves in the plasmasphere. In [7] a numerical solution of a system of nonlinear equations describing parametric interactions between LOR and ELF pump waves excited in the TPBL by the diamagnetic ion currents and hot ion ring instabilities [8, 9] was analyzed. Obtained results show that nonlinear coalescence of the LOR and ELF waves leads to oblique electromagnetic VLF (whistler) emissions at frequencies much greater than the LH resonance frequency, in agreement with the observations. Finally Particle-In-Cell (PIC) simulation of parametric generation of electromagnetic whistler waves will be discussed. This simulation will be initiated by excitation of the forced wave electric field at VLF and ELF frequencies. Such initiation is possible due to the ability of the PIC code known as Large Scale Plasma (LSP) code [10] to excite traveling plane waves in a simulation box. Wave vectors and frequencies of excited in this way

modes are chosen to satisfy the ELF and VLF dispersion relations. It was demonstrated that quasi-electrostatic VLF and electromagnetic ELF waves in the process of nonlinear interaction were able to excite electromagnetic whistler waves. These results was obtained implementing a Lagrangian fluid model – part of the LSP package. Simulation results also reveal generation of multiple sideband emissions around the pump VLF wave. These simulation results strongly support analytical model presented in [1, 2] and used in [6, 7] to explain the observations of whistler waves in the plasmasphere boundary layer [11].

2. VLF waves in the ionosphere

We analyze excitation of waves with frequencies ω several times above the lower hybrid resonance frequency, but below the one half of electron cyclotron frequency *i.e.*:

$$\omega_{LH} < \omega < \frac{1}{2}\omega_{ce},\tag{1}$$

where the lower hybrid frequency ω_{LH} in the case when $\omega_{ce}^2 << \omega_{pe}^2$ is given by:

$$\omega_{LH}^2 = \frac{\omega_{pi}^2}{1 + \omega_{pe}^2/\omega_{ce}^2}.\tag{2}$$

and ω_{pe} is an electron plasma frequency. It is well known that in this case in a cold plasma only one mode can be excited. The character features of excited wave field at large distances from the source region can be explained using a plot presented at **Figure 1**. This plot is similar to the commonly used wave refractive index surface plot. The plot at **Figure 1** was obtained using the dispersion relation of VLF waves presented below:
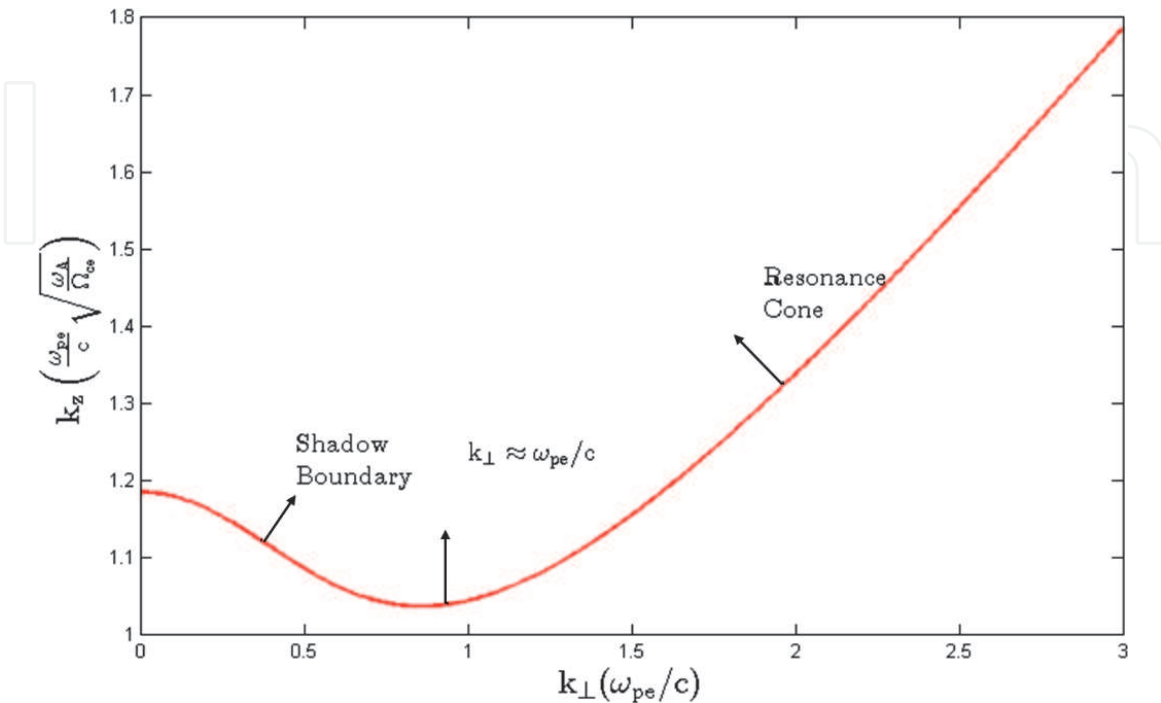
Figure 1.
Wave number surface for a constant $\omega_{LH} < \omega < \frac{1}{2}\omega_{ce}$ with three critical points.

$$\omega^2 = \frac{m_i}{m_e} \frac{k_z^2}{k^2} \frac{\omega_{LH}^2}{\left(1 + \frac{\omega_{pe}^2}{k^2 c^2}\right)^2} \tag{3}$$

In (3) the wave vector k is defined as $k^2 = k_\perp^2 + k_z^2$ where $k_\perp$ and k_z are the wave vector components perpendicular and along an external magnetic field. In **Figure 1** the wave vector component k_z along the magnetic field is plotted versus $k_\perp$ assuming a constant ω. Most of the radiated by an antenna power can be found in a region in k space occupied by the quasi-electrostatic whistler waves with the parameter $\omega_{pe}^2/k^2 c^2 \leq 1$. Another part of the wave spectrum in k space which satisfies the condition $\omega_{pe}^2/k^2 c^2 >> 1$ belongs to the electromagnetic whistler waves and is radiated up to an angle 19.5° in oblique direction. This is the shadow boundary determined by the long wavelength inflection point and radiated power of these waves is small compared to the power radiated into the quasi-electrostatic part of the wave spectrum.

In [12] it was shown that most of the wave power is radiated perpendicular to the curve presented in **Figure 1** and depends from the distance as R^{-1} except three critical points which define three directions. Two of them are inflection points $d^2 k_z/dk_\perp^2$. In these points a wave field dependence is given as $R^{-5/6}$. The third critical point is defined from the equation $d^2 k_z/dk_\perp^2 = 0$ and provides wave field dependence in the form $R^{-1/2}$ and corresponds to the wave power radiated along the direction of magnetic field.

3. Parametric excitation of VLF waves in the ionosphere

Nearly monochromatic signals injected from ground-based VLF transmitters are known to experience bandwidth expansion as they traverse the ionosphere [13–17] and magnetosphere [18]. Several mechanisms have been proposed to explain this phenomenon based upon linear and nonlinear scattering assuming existence of magnetic-field-aligned plasma density irregularities. In the absence of ionosphere irregularities a mechanism based on a parametric instability was proposed in [19–21].

Reports on sideband signals associated with VLF transmitter signals are rather scarce. Spectral peaks have been identified near the magnetic equatorial plane on the ISEE satellite at approximately ±55 Hz of the carrier frequency (13.1 and 13.6 kHz) of Omega pulses [22]. Similar peaks seem to be observed on the COS-MOS 1809 satellite and generated in the ionosphere by the carrier frequency 19 kHz [17]. Sidebands at approximately ±500 Hz of the carrier frequency (11.9 and 12.65 kHz) of Alpha pulses have been observed in the ionosphere by the AUREOL 3 satellite [3, 4].

At first sight, the 50-Hz sidebands observed on AUREOL 3 seem to correspond the Riggin and Kelly [19] prediction in which the transmitted wave decays into a lower hybrid wave and an ion-acoustic type of oscillation. To account for the existence of two symmetric spectral peaks, one may replace the three-wave parametric instability considered by these authors by a four-wave parametric instability (or modulation instability) as suggested in [21]. According to this scheme, the ELF branch is due to a purely growing electrostatic mode with wave vector ***k*** large enough to provide sidebands ±|kV_s| off the transmitter frequency.

(V_s is the satellite velocity). This mode is excited in course of a four-wave process by the incident VLF transmitter wave. In our case, the ELF wave branch is
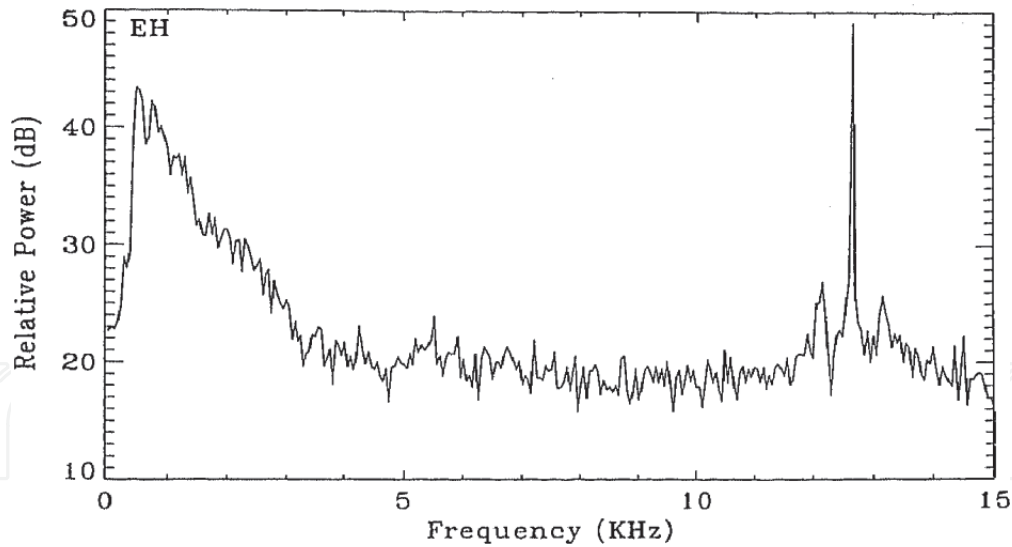
Figure 2.
Averaged power spectral density of electric field. ELF natural emission at 500 Hz, VLF transmitted emission at 12.65 kHz, sidebands at frequencies (12.65 + 0.5) kHz and (12.65−0.5) kHz. This data were observed in ionosphere on AUREOL 3 satellite during experiments in framework of ARCAD project [3].

clearly electromagnetic and as such is of natural origin. Therefore, another explanation in accord with this experimental data has to be found.

Sotnikov et al. [1] proposed another mechanism for the production of 500-Hz sidebands. It is based on nonlinear coupling between the transmitted wave and the ELF emission above the local proton gyrofrequency. The sidebands are shown to be forced oscillations, excited only where the coupling take place. We consider the nonlinear coupling model described in the articles [1, 2].

Next, analysis of the parametrically generated VLF turbulence has been developed in the articles by Sotnikov et al., [1, 2] as attempt to explain appearance of symmetric sidebands in frequency. Such parametrically generated waves were observed in multiple ionospheric experiments. In these experiments two types of waves were present, waves excited by a VLF transmitter and ELF waves excited due to natural processes in the ionosphere. It was demonstrated that beat wave excitation mechanism can be responsible for appearance of observed sidebands with comparable wave amplitudes. Sidebands were excited at combination frequencies given by:

$$\omega_{\pm} = \omega_{k_1} \pm \omega_{k_2},$$ (4)

which can result in sideband emissions. The sideband wave numbers are matched according to

$$k_{\pm} = k_1 \pm k_2$$ (5)

Note that sidebands are not plasma eigenmodes but forced oscillations excited only where VLF to ELF wave coupling take place (**Figures 2** and **3**).

Using the cold plasma approximation the equations for the perpendicular to magnetic field sideband electric field components can be derived in the form [2]:

$$E_{\perp k_+} = \frac{e}{2m} \frac{k_+}{\Omega_e \delta\omega_+} [E_{k_1} \times E_{k_2}]_z$$
$$E_{\perp k_-} = \frac{e}{2m} \frac{k_-}{\Omega_e \delta\omega_-} [E_{k_1} \times E_{k_2}]_z$$ (6)
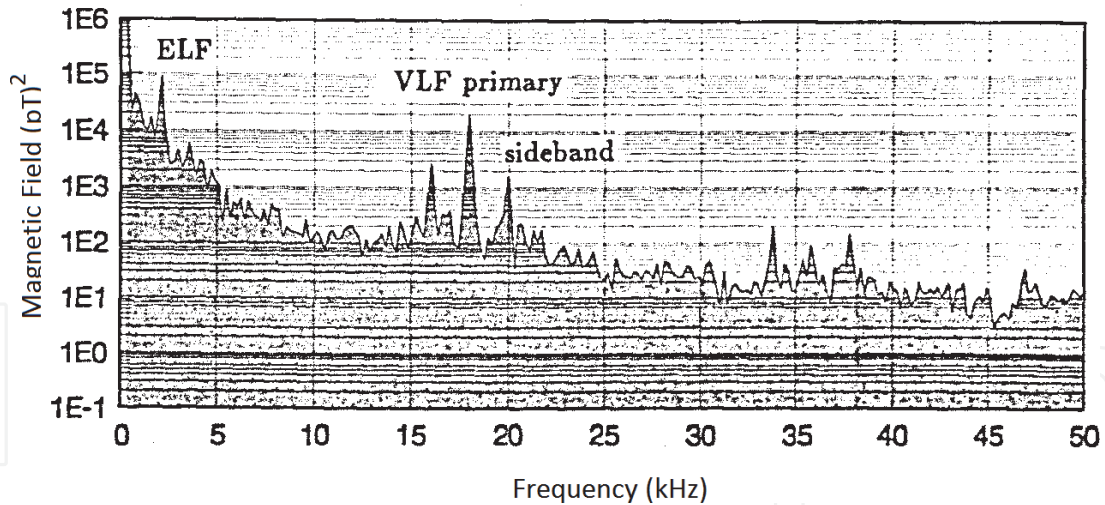
Figure 3.
ELF natural emission at 2 kHz, VLF transmitted emission at 17.95 kHz, sidebands at frequencies (17.95 + 2) kHz and (17.95–2) kHz. This data were observed during cooperative high-altitude rocket gun experiment (CHARGE 2B) carried out in march 1992.

where

$$\frac{\delta\omega_{\pm}}{\Omega_e} = \frac{k_{z1}/k_1}{1 + \omega_{pe}^2/(k_1^2 c^2)} \pm \frac{k_{z2}/k_2}{1 + \omega_{pe}^2/(k_2^2 c^2)} - \frac{(k_{z1} \pm k_{z2})/k_{3\pm}}{1 + \omega_{pe}^2/(k_{3\pm}^2 c^2)}, \qquad (7)$$

$k_{3\pm}^2 = k_1^2 + k_2^2 \pm 2k_1 k_2 \cos(\theta)$ and θ is the angle between **k** vectors.

Sidebands may be a result of nonlinear coupling of the VLF transmitter wave and the natural ELF emission above the local proton gyrofrequency. The VLF wave propagate through the ionosphere as a whistler mode.

$$\omega_{k_1} = \Omega_e \frac{k_{1z}/k_1}{1 + \omega_{pe}^2/(k_1^2 c^2)} \qquad (8)$$

For the transmitted frequency $\omega/2\pi = 12$ kHZ, the corresponding wave number is $k_1 \approx 2 \cdot 10^{-4}$cm^{-1}. For the known parameters whistler propagates with $\omega_{pe}^2/k_1^2 c^2 = 1$ at large angle to the magnetic field.

The characteristic frequency ω_{k_z} of the ELF wave is slightly above the ion gyrofrequency and $k_2 \approx 3 \cdot 10^{-5}$ cm^{-1}. These waves generally propagate at large angle to the geomagnetic field. As $\omega_{pe}^2/k_2^2 c^2 >> 1$, it is described by

$$\omega_{k_2} = \Omega_e \frac{k_{2z}}{k_2} \frac{k_1^2 c^2}{\omega_{pe}^2}, \qquad (9)$$

where Ω_e is the electron cyclotron frequency.

4. Excitation of whistler waves in a turbulent plasmapause boundary layer

In this section we will discuss parametric interaction of quasi-electrostatic lower oblique resonance waves excited by electron and ion diamagnetic currents and hot anisotropic ion distributions [6–9, 23, 24] with ELF waves in the turbulent

plasmasphere boundary layer (TPBL). It is demonstrated below that this nonlinear mechanism can be responsible for generation of broadband, oblique Very Low Frequency (VLF) whistler (W) waves at frequencies much greater than the LH resonance frequency. It is important because the well known whistler generation mechanism by energetic electrons is unavailable in the TPB. Below we present the results of numerical solution of a system of nonlinear equations describing parametric interactions between LOR and ELF pump waves excited in the TPBL by the diamagnetic ion currents and hot ion ring instabilities [8, 9]. Due to instabilities the LOR and ELF waves are generated. Results of simulation confirm that due to nonlinear interaction electromagnetic whistler waves propagating in oblique direction are excited. The frequency of excited waves is well above the Lower Hybrid frequency what is in agreement with experimental results.

In general, parametric interaction of two waves, ω_{k_1} and Ω_{k_2}, produces sidebands at the combination frequencies, $\omega_\pm$, that satisfy the matching conditions (4) and (5). In the case in question, we have $\omega_\pm \approx \omega_{k_1} >> \Omega_{k_2}$, that is, the high-frequency (VLF) and low-frequency (ELF) counterparts, with $|k_\pm| << |k_1| \approx |k_2|$. A general approach for solution of this problem was developed to explain symmetric sidebands, observed during active experiments with injection of a high-power VLF pump whistler wave [1] and modulated electron beam [2] into the ionosphere. It was demonstrated that beat wave interaction between the artificially excited VLF wave and natural ELF emissions can produce observed VLF sidebands. This can be viewed as a first step in the process of a broad VLF spectrum formation because subsequent interaction produces secondary sideband waves and this process continues until the broad range of wavenumbers in k-space is excited. This leads to the requirement that analytical description of the problem should be capable to correctly capture nonlinear interaction in the broad range of wavenumbers and wave frequencies.

In [1, 2, 6, 25] equations written in the Fourier space were used and it was sufficient for obtaining the estimate for sideband amplitudes. To study a nonlinear stage of excited wave turbulence we will switch from the Fourier analysis to description in time and space. To do so Maxwell's equations together with equations of motion of magnetized electrons and unmagnetized ions in hydrodynamic approximation will be used. It is well known that to describe correctly nonlinear evolution of VLF turbulence it is necessary to use 3D description [26–28]. We will use two different systems of equations for description of ELF and VLF waves. They are connected through nonlinear terms containing vector nonlinearities. As a result of cumbersome but straightforward manipulations as in [1, 2, 25], we can obtain nonlinear set of equations for parametric interaction of the VLF and ELF waves, which can be found in [7]. The resulting system of nonlinear equations which describes evolution of VLF turbulence and appearance of electromagnetic whistler waves was solved numerically. Using the developed FORTRAN code which employs the predictor–corrector quasi-spectral numerical scheme detailed analysis of nonlinear mechanism of electromagnetic whistler wave generation from the quasi-electrostatic LOR wave spectra was demonstrated. Main results of this analysis can be found in [25, 29].

Numerical analysis was carried out in a simulation box with the grid size 256 x 32 x 128. In the x direction it includes 16 VLF wavelengths, in the y direction 2 ELF wavelengths and in the z direction 1 ELF wavelength, what corresponds to 4 VLF wavelengths. In all directions periodic boundary conditions were applied.

An initial value problem was solved with VLF and ELF pump waves turn-on all the time. The adaptive time stepping was implemented with initial dimensionless time step $\Delta \bar{t} = 2\pi \cdot 10^{-2} (\Delta t \approx 10^{-5}$ s$)$. The computation takes a few days on a standard PC. The input conditions are taken close to the observed values in the plasmasphere [23]:

$B_0 = 0.003$ G, $n_0 = 10^2$ cm^{-3}, $\omega_{ce} = 5.3 \cdot 10^4$ s^{-1}, $\omega_{pe} = 5.6 \cdot 10^5$ s^{-1} and $\omega_{LH} \approx 1.2 \cdot 10^3$ s^{-1}. The input VLF pump wave is a monochromatic quasi-electrostatic LOR wave at $\omega_1 \approx 5\omega_{LH}$, 3-D wavevector $k_1 = \frac{\omega_{pe}}{c}(8, 0, 0.94\mu^{-1/2})$, and the amplitude $E_1 = 2$ mV/m . The input ELF wave is a monochromatic MS wave wit h$\Omega_2 \approx 0.77$ ω_{LH}, $k_2 = \frac{\omega_{pe}}{c}(0, 0.05, 0.13\mu^{-1/2})$, and $E_2 = 2$ mV/m. The values of ω_1 and k_1, as well as Ω_2 and k_2, satisfy the dispersion equation for Fast Magnetosonic (FMS) waves:

$$\omega_k^2 \approx \frac{\omega_{LH}^2}{1 + \frac{\omega_{pe}^2}{k^2 c^2}}\left[1 + \frac{M}{m}\frac{k_z^2}{k^2}\frac{1}{1 + \frac{\omega_{pe}^2}{k^2 c^2}}\right]$$

Note that the pump wave parameters are chosen specifically so that they are close to but not exactly satisfy the resonance conditions (Eq. (3)) required to get the maximal efficiency of parametric interaction, as described in [1, 2]. However, in the resonance case, the collisionless system of nonlinear equations crashes after only a few time steps because of singularities that cannot be avoided, unless collisional terms are included. Spatial spectra in 2D of the electrostatic potential $\delta\Phi$ of nonlinearly excited VLF waves (frames b, c, and d) and a pump wave Φ_0 (frame a) are presented in **Figure 4**. They were taken in the middle of the computational box (y = 16) at 10^{-3}, 0.1, and 0.18 sec from the beginning of the computational run. Presented in **Figure 4** results clearly demonstrate that the spectral density of electromagnetic modes with $kc << \omega_{pe}$ absent initially starts to grow with time due to the wave cascade towards smaller wavenumbers. Eventually we find that electromagnetic VLF whistlers with frequencies from the range $3 < \omega/\omega_{LH} < 7.5$ produce noticeable part of the excited wave spectrum. The wavenumbers of these waves are inside the rectangles in **Figure 4b–d**. These waves represent the long wavelength part of the dispersion relation for the FMS waves, which corresponds to an electromagnetic VLF whistler wave. Calculations were initiated with $k_\perp \approx k_x >> k_y$. Time evolution of oblique electromagnetic VLF whistler waves with the wavenumbers
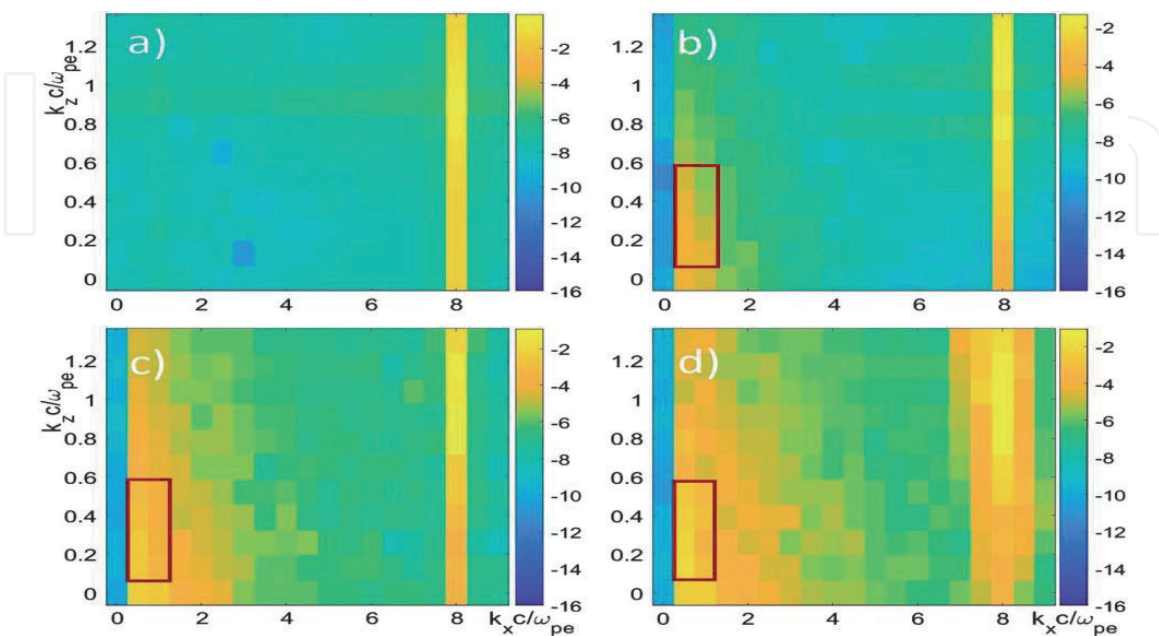
Figure 4.
(a) – 2D representation of the VLF pump wave in Fourier space. (b) – 2D Fourier spectra of VLF density perturbations at time T_1. *(c) - 2D Fourier spectra of VLF density perturbations at time* $96 \cdot T_1$. *(d) -2D Fourier spectra of VLF density perturbations at time* $171 \cdot T_1$.
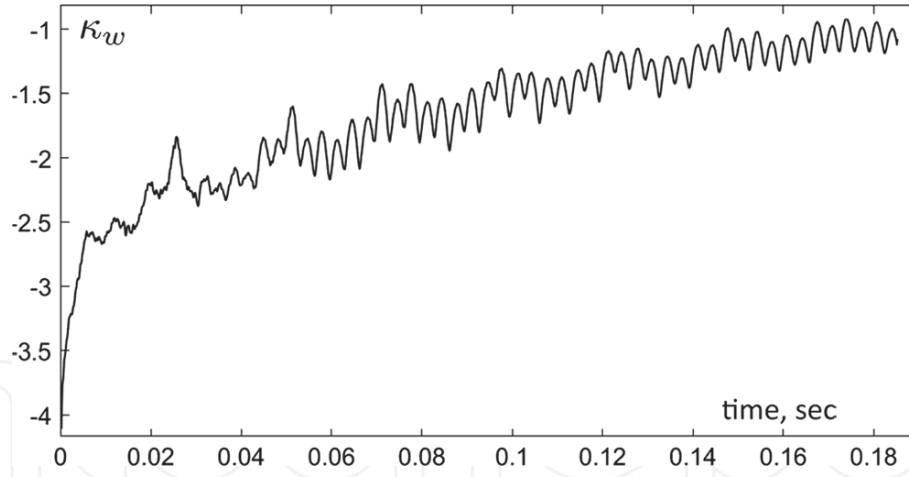
Figure 5.
The whistler generation efficiency, $\kappa_w \approx (\omega_{ce}/2\omega_w)^{1/2} E_w/E_{LH}$ in logarithmic scale versus time.

from the rectangles in **Figure 4** is presented in more details in **Figure 5**. It shows the change in time of efficiency of wave transformation from quasi-electrostatic to an electromagnetic part of the wave spectra $\kappa_w \approx (\omega_{ce}/2\omega_w)^{1/2} E_w/E_{LH}$. The root of the mean-square amplitude of the quasi-electrostatic VLF wave field energy density is denoted as E_{LH} whereas E_w represents an electromagnetic wave energy density inside the rectangles. Numerical results show that the amplitude of electromagnetic whistler waves increases with time and eventually reaches the value $\sim 0.1 E_{LH}$. It is worth mentioning that the analytical estimate presented in [6] provides similar values and is also consistent with the experimental data. Presented numerical results allow to implement the following scenario of electromagnetic VLF whistler waves generation based on beat wave excitation mechanism. A VLF pump wave in the process of nonlinear interaction with an ELF pump wave generates sideband waves, which in turn generate another sidebands and spread of the wave spectrum in k-space. This in turn leads to appearance of long wavelength waves corresponding to an electromagnetic whistlers. Amplitudes of these waves rapidly grow and can achieve very large values, up to the 30% of the quasi-electrostatic pump wave amplitudes.

In (a) – (d) electromagnetic VLF density perturbations with frequencies from the interval $3 < \omega/\omega_{LH} < 7.5$ are placed inside a rectangle. To the right of each panel one can find color codes in logarithmic scale representing normalized wave amplitudes. Numerical setup with constant in time pump waves amplitudes was used. Chosen pump waves did not obey resonance conditions for sideband excitation and this resulted in relatively small sideband amplitudes. This is the reason it takes so much time to form a broad VLF wave spectrum presented in **Figure 4**. This in turn leads to relatively slow growth of VLF type perturbations. Numerical results also show that nonlinearly excited ELF perturbations does not contribute much to VLF perturbations.

This conclusion follows from the comparison with the results of simulations with exactly the same input parameters but without taking account of the ELF disturbance.

These waves have also been detected in the TPBL, which is devoid of substorm-injected kiloelectronvolt electrons [11, 22]. These emissions represent a distinctive subset of the substorm/storm-related VLF whistler activity and provide the rate of pitch angle diffusion of the radiation belt (RB) electrons that can explain the plasmapause-radiation belt boundary correlation [11]. As the "standard" whistler generation mechanism by energetic electrons is unavailable in the TPBL, [6]

suggested nonlinear interactions between quasi-electrostatic LH oblique resonance (LOR) and ELF waves to be the source.

Free energy for enhanced waves comes from electron diamagnetic currents in the entry layer near the TPBL's outer boundary [6, 22], while diamagnetic ion currents and anisotropic (nearly ring like) hot ion distributions are the main contributors near the inner boundary [8, 9]. It is worth mentioning that electromagnetic VLF whistler waves with frequencies far exceeding the Lower Hybrid frequency were produced as a result of numerical solution of nonlinear equations describing interaction of quasi-electrostatic lower oblique resonance (LOR) waves and externally excited ELF waves. This result supports the suggestion that experimentally detected in the TPBL electromagnetic VLF whistler waves with frequencies well above the Lower Hybrid frequency can be produced in the process of nonlinear interaction between the LOR and ELF waves. Experimental results also show that one of the possible mechanisms for changes in the outer radiation belt boundary is connected with the presence of electromagnetic VLF whistler waves. Taking into account that due to the absence of substorm-injected kiloelectronvolt electrons the well known whistler generation mechanism is not applicable to the plasma sheet inner boundary, we can conclude that described above nonlinear generation mechanism can play an important role in this region. This statement is also supported by observations.

5. Parametric excitation of whistler waves: LSP simulation results

A well-developed particle-in-cell plasma simulation code called Large Scale Plasma (LSP) [10] was used to perform 3D simulations of VLF field excitation. We have used the Large Scale Plasma (LSP) simulation code to force the VLF and ELF modes in a cold, magnetized plasma. One of the built in LSP models is the Lagrangian fluid model for both the ion and the electron species. This model was used to obtain presented results. Fluid particles in the model carry the fluid velocity. It is updated every time step with the help of the momentum equation. The fluid particles characteristics such as velocity and position are weighted on the simulation grid. This allows to involve the source terms which define excited electromagnetic fields through supplied density and current density. In addition, using the known density and fluid velocity an equation for temperature can also be solved on the grid. In this model plasma pressure can also be found on the grid assuming an ideal gas approximation. Next, the pressure gradient on the grid can be used in the momentum equation to update the particle velocities and fields. To allow for larger spatial grids and simulation time steps in LSP an implicit energy conservation scheme is used. In this way the scheme provides the Lorentz force push. Electric and magnetic fields are solved self-consistently. This approach allows to substantially reduce simulation time in comparison with implementation of the explicit field solvers. The initial distribution function is assumed to be Maxwellian to allow plasma to behave as an ideal gas.

Simulations to compare the Lagrangian model with the fully PIC results with application to the nonlinear interaction of VLF and ELF waves restricted by 2D approximation were carried out. Obtained results were very close and this was the reason the Lagrangian approach was used. This approach due to the dramatic reduction of simulation time allowed to perform 3D simulations what is necessary to obtain correct nonlinear description of parametric interaction. There are several other advantages in using a Lagrangian fluid approach. Fewer particles per cell are needed and simulations are much quieter. In presented simulations only eight particles per cell were used. To obtain similar quality result using a fully kinetic

approach it was needed to use 200 particles per cell. To carry out simulations a 3D Cartesian geometry was used with imposed externally magnetic field directed along a z axis. The amplitude of the magnetic field was chosen to be 0.3 G and plasma density $\sim 10^5$ cm^{-3} what corresponds to the ionospheric parameters. In simulations hydrogen ions with a mass ratio of 1836:1 were used. An outlet boundary conditions were used and the wave was allowed to propagate out of a simulation box minimizing reflections and wave return back into the simulation box. In a cold plasma used in simulations no thermal expansion was observed and no particles were leaving a simulation box.

In LSP we can impose a traveling plane wave inside a simulation box. Both VLF and ELF waves are excited simultaneously. We choose k_x, k_y and ω. We then use the VLF and ELF dispersion to solve for k_z for these waves. Therefore, unlike the waveguide approach which excites a seemingly random set of k-vectors consistent with the dispersion relation, we can target any mode we desire. Because we are directly exciting specific modes, we call this method the "Direct Excitation" (DE) method. The boundary conditions are also much simpler using the DE method. We have chosen to use outlet boundaries. The waves are free to leave the simulation domain and there is little reflection of the waves at the boundaries. Finally, the simulation domain is much smaller, which allows is to make the plasma region larger and therefore resolve smaller k-vectors. Lastly, because we can target specific k-vectors, using the DE method we can test the theory and compare results from LSP with the direct solution to the equations which describe the parametric interaction. The following k-vectors and frequencies are used in the simulation results shown below: $k_{VLF} = (3.5, 0, 1.1)\omega_{pe}/c$ and $k_{ELF} = (0.1, 0.1, 0.11)\omega_{pe}/c$. The ELF and VLF frequencies are $0.8\omega_{LH}$ and $12\omega_{LH}$. This set of parameters leads to $\delta\omega_+ \approx 0.013\omega_{LH}$ and $\delta\omega_- \approx 0.05\omega_{LH}$. Therefore, we expect the positive sideband to be a larger amplitude since $\delta\omega_+$ is smaller than $\delta\omega_-$ and therefore closer to resonance. Indeed, we have seen that the positive sideband is often a larger amplitude. The simulation was run for $\sim$11 ELF periods. The VLF and ELF waves are exciting by specifying the y-component of the electric field only. This leads to the excitation of the other electric field components and the magnetic field. Note that we do not specifically excite B_y. Therefore all field components are excited self-consistently when only one field component is excited. The black curves in **Figure 6** represent the solutions to the VLF and ELF dispersion equations. The most prominent modes occur at the wavenumbers which are driven externally. The VLF dispersion curve
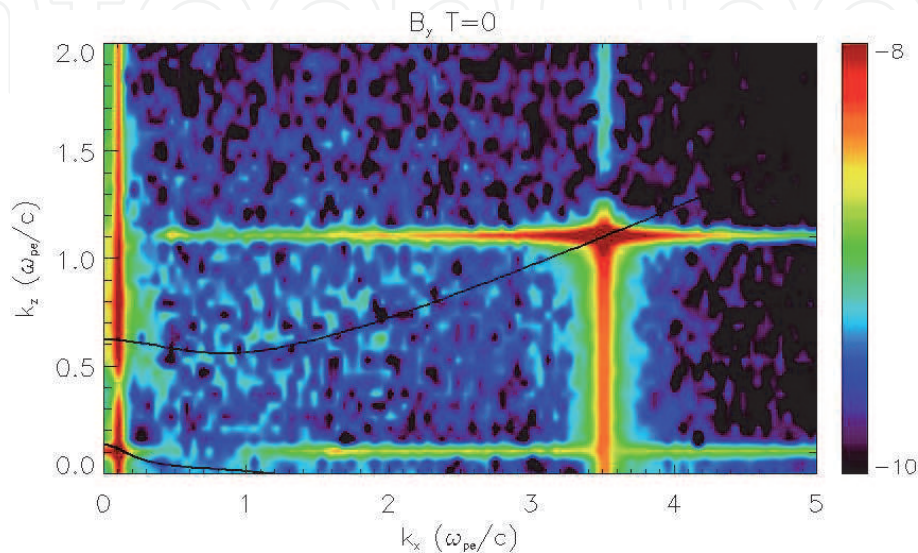
Figure 6.
VLF/ELF wave power spectra of magnetic field component by at t = 0.
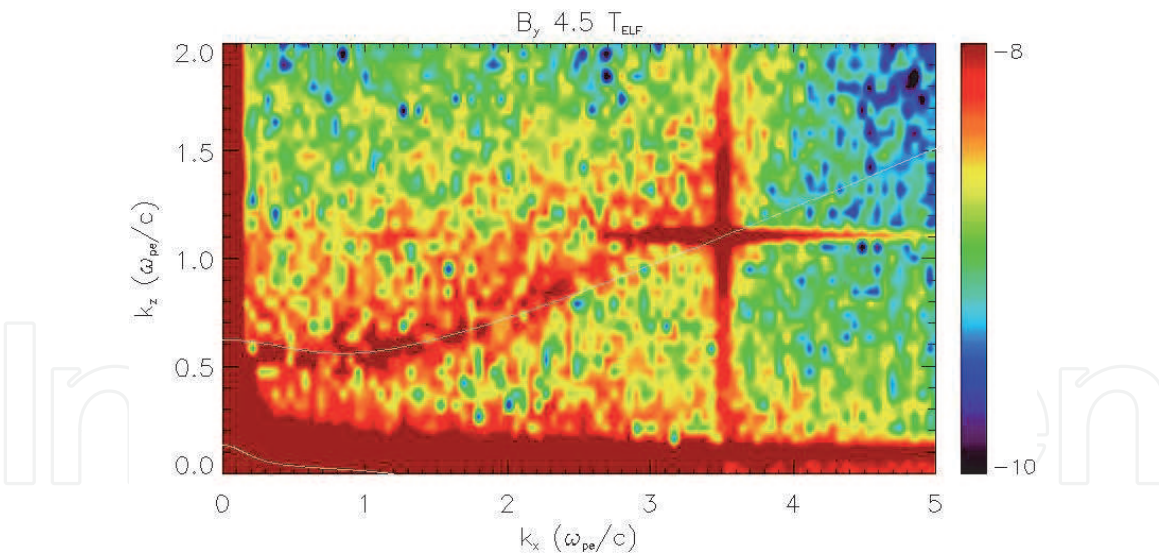
Figure 7.
*VLF/ELF wave power spectra of the magnetic field component B_y at time $t = 4.5 \times T_{ELF}$. Wave power spectra presented at $t = 4.5 \times T_{ELF}$ are consistent with the VLF dispersion relation presented in **Figure 1**. This simulation result confirms nonlinear transformation of a quasi-electrostatic LOR to an electromagnetic VLF whistler waves.*

crosses the externally driven VLF k-vector and ELF dispersion crosses the externally driven ELF k-vector. Therefore, we are confident that we are driving the correct modes (**Figure 7**).

6. Conclusion

In this Chapter using analytical methods and PIC simulation we analyzed efficiency of excitation of electromagnetic VLF whistler waves due to parametric interaction of quasi-electrostatic LOR and ELF waves in the ionospheric plasma.

$\delta\omega_{\pm} << \Omega_{k_s}$ and values of the sideband amplitudes in agreement with experimental results. It is also possible to satisfy the condition for resonance excitation of VLF waves. If we take into account resonance broadening $\Delta\omega$ due to finite collisions then $\Delta\omega \sim \frac{\omega}{\omega_{ce}}\nu$, where ν is the collision frequency. This means that for nonresonant excitation of sidebands to occur $\delta\omega_{\pm} > \Delta\omega$ must be satisfied. In the opposite case when $\delta\omega_{\pm} < \Delta\omega$ resonant excitation mechanism takes place.

A numerical model describing nonlinear parametric coupling of LOR with ELF waves in cold collisionless plasma has been developed in order to explain the generation of electromagnetic VLF whistler waves in the TPBL in the absence of energetic electrons. These electrons are usually viewed as a source for generation of electromagnetic VLF whistler waves and absence of them in the satellite data was an unanswered question for understanding of a generation mechanism. The results of the 3D LSP simulation confirm that nonlinearly excited waves exhibit spectral features consistent with the observed electromagnetic VLF whistler waves.

Using PIC simulations we have directly tested the nonlinear mechanism suggested in [6] by forcing a quasi-electrostatic whistler wave (i.e., a LOR wave) and an ELF mode to allow parametric interaction. Obtained simulation results confirm that this generation mechanism is capable to explain observed electromagnetic VLF modes. Simulation results clearly show that the LOR mode has cascaded to lower wave number electromagnetic VLF whistler modes. Therefore, the model proposed in [6] that the observed whistler waves are due to a parametric interaction

between the LOR and ELF waves is consistent with the findings from the simulation results.

Acknowledgements

Author details

Vladimir I. Sotnikov
Air Force Research Laboratory, Sensors Directorate, Wright-Patterson AFB, OH, USA

*Address all correspondence to: vladimir.sotnikov.1@us.af.mil

IntechOpen

References

[1] Sotnikov V. I., Fiala V., Lefeuvre F., Lagoutte D., and Mogilevskii M., Excitation of sidebands due to nonlinear coupling between VLF transmittesr signal and a natural ELF emission, J. Geophys. Res. 1991; 96, 11363-11374, DOI:10.1029 /91JA00695

[2] Sotnikov V.I., Schriver D., Ashour-Abdalla M., and Ernstmeyer J., Excitation of sideband emissions by a modulated electron beam during the CHARGE 2B mission, J. Geophys. Res. 1994; 99, 8917-8926, DOI:10.1029/ 93JA03024

[3] Tanaka, Y., Lagoutte, D., Hayakawa, M., Tajima, M.S., Geophys. Spectral broadening of VLF transmitter signals and sideband structure observed on Aureol 3 satellite at middle latitudes, J. Geophys. Res. 1987; 92,7551-7561

[4] Lagoutte D., Lefeuvre, F., Hanasz, J., Application of bicoherence analysis in study of wave interactions in space plasma, J. Geophys. Res. 1989; 94, 435-442

[5] Myers, N.B., and Ernstmeyer, J., Notes on the CHARGE 2B electron beam experiment platform, Tech. Memo. RL TM-92-28, Utah State University, Logan, Utah, 1992.

[6] Mishin, E.V., and Sotnikov, V.I., The turbulent plasmasphere boundary layer and the outer radiation belt boundary, Plasma Phys. Control. Fusion 2017; 59, 124003-124012

[7] Mishin E.V., Sotnikov V.I., Gershenzon N., and Amit Sharma, Whistler Waves in the Plasmasphere Boundary Layer: Nonlinear Parametric Excitation, Geophys. Res. Letters 2019; 10.1029/2019GL083432, 1-6

[8] LaBelle, J., Treumann, R., Current-driven lower hybrid waves at the inner edge of the ring current; Journal of Geophysical Research 1988; 93, 2591–2598.

[9] Mishin, E., Burke, W., Storm time coupling of the ring current, plasmasphere and topside ionosphere: Electromagnetic and plasma disturbances, Journal of Geophysical Research 2005; 110, A07209. DOI: 10.1029/2005JA011021

[10] Welch D.R., Rose V., Cueno M.E., Campbell, R.B. and Mehlhorn T.A., Integrated Simulation of the generation and transport of proton beams from laser-target interaction, Phys. Plasmas 2006; 14, 25-35

[11] Mishin, E., Albert, J., & Santolik, O., SAID/SAPS-related VLF waves and the outer radiation belt boundary. Geophysical Research Letters 2011; 38, 21101-21109, DOI: 10.1029/ 2011GL049613

[12] Fisher R.K. and Gould R.W., Resonances cones in the field pattern of a radio frequency probe in a warm anisotropic plasma, Phys. Fluids 1971; 857-865

[13] Bell T.F., James, H.G., Inan, U.S., Katsufrakis, J.P., The apparent spectral broadening of VLF transmitter signals during transionospheric propagation. J. Geophys. Res. 1983; 88, 4813 - 4821

[14] Titova E.E., Di, V.I., Yurov, V.E., Raspopov, O.M., Trakhtengertz, V.Yu., Jiricek, T., Triska P., Interaction between VLF waves and the turbulent ionosphere. Geopys. Res. Lett. 1984, 11, 323-331

[15] Inan U.S., Bell, T.F., Spectral broadening of VLF transmitter signals observed on DE 1: A quasi-electrostatic phenomenon, J. Geophys. Res. 1985; 90, 1771-1783

[16] Tanaka, Y., Lagoutte, D., Hayakawa, M., Tajima, M.S., Spectral

broadening of VLF transmitter signals and sideband structure observed on Aureol 3 satellite at middle latitudes, J. Geophys. Res. 1987; 92,7551-7562

[17] Chmyrev V.M., Parametric excitation of ELF waves and acceleration of ions during the injection of strong VLF waves into ionospher, Kosm. Issled. 1989; 27, 249-263

[18] Bell T.F. and Ngo, H.D., Electrostatic waves stimulated by coherent VLF signals propagating in and near the inner radiation belt. J. Geophys. Res. 1988; 93, 2599-261

[19] Riggin, D. and Kelley, M.C., The possible production of lower hybrid parametric instabilities by VLF ground transmitters and by natural emissions, J. Geophys. Res. 1982; 87, 2545-2553

[20] Lee M.C. and Kuo, S.P., Production of lower hybrid waves and field-aligned plasma density striations by whistlers, J. Geophys. Res. 1984; 89, 10873-10885

[21] Groves K.M., Lee, M.C., Kuo, S.P., Spectral broadening of VLF radio signals traversing the ionosphere, J. Geophys. Res. 1988; 93, 14, 683-697

[22] T. F. Bell, J. Geophys. Res. 1985; 90, 2792-2802, DOI: 10.1029/ JA090iA03p02792

[23] Mishin, E., Interaction of substorm injections with the subauroral geospace: 1.Multispacecraft observations of SAID, Journal of Geophysical Research: Space Physics 2013; 118, 5782–5796, DOI: 10.1002/jgra.50548

[24] Mishin, E., Puhl-Quinn, P. A., & Santolik, O. (2010). SAID: A turbulent plasmaspheric boundary layer. Geophysical Research Letters 2010; 37, L07106, DOI: 10.1029/2010GL042929

[25] Sotnikov, V., Kim, T., Caplinger, J., Main, D., Mishin, E., Gershenzon, N., Parametric excitation of very low frequency (VLF) electromagnetic whistler waves and interaction with energetic electrons in radiation belt. Plasma Physics and Controlled Fusion 2018; 60, 7-14, DOI: 10.1088/1361-6587

[26] Ganguli, G., Rudakov, L., Scales, W., Wang, J., & Mithaiwala, Three dimensional character of whistler turbulence, Physics of Plasmas 2010; 17, 52310-52321, DOI: 10.1063/1.3420245

[27] Shapiro, V., Shevchenko, V., Solov'ev, G., Kalinin, V., Bingham, R., Sagdeev, R., Wave collapse at lower-hybrid resonance, Physics of Fluids, 1993; 5, 3148–3162.

[28] Sotnikov V., Shapiro V., Shevchenko V., Macroscopic consequences of collapse at the lower hybrid resonance. Soviet Journal of Plasma Physics 1978, 4, 252–257.

[29] Sotnikov V.I., Ivanov V.V., Presura R., Leboeuf J.N., Onishchenko O.G., Oliver B.V., Jones B., Mehlhorn T.A., Deeney C., Investigation of Compressible Electromagnetic Flute Mode Instability in Finite Beta Plasma in Support of Z-pinch and Laboratory Astrophysics Experiments, Commun. Comput. Phys. 2008; 4, 611–623